The Use of Two Reactive Elements to Optimize Oxidation Performance of Alumina-Forming Alloys

B. A. Pint, K. L. More and I. G. Wright
Metals and Ceramics Division
Oak Ridge National Laboratory
Oak Ridge, TN 37831-6156

Abstract

Standard reactive element (RE) studies have characterized the behavior of single RE additions such as Y, La or Hf. However, several commercial alumina-forming alloys are "co-doped" with two or more RE additions which allows the total amount of RE dopant in the alloy to be reduced. The oxidation performance of both commercial and laboratory-made co-doped alloys shows better scale adhesion and/or slower scale growth rates than comparable alloys with one RE addition. Characterization of the alumina scales showed no significant change in the grain structure with co-doping; however, as the total RE addition was reduced in co-doped alloys, a smaller volume of RE-rich oxides was observed within the scale. Quantification of the amount of RE ionic segregation on alumina scale grain boundaries formed on single doped and co-doped alloys showed similar amounts of segregation.

Introduction

The effects of reactive element (RE) additions (e.g. Y, Zr, Hf, La, Ce, etc.) has been widely studied for more than 65 years[1-7] but has been a special focus of attention for the past 25 years because of the interest in developing corrosion resistant alloys that form protective alumina scales. For chromia-forming alloys, a RE addition is not necessarily needed for adequate oxidation resistance. However, for alumina forming alloys, a RE addition imparts such a strong benefit on spallation resistance that most commercial alumina-forming alloys contain either a RE alloy addition or an RE oxide dispersion.

When the corrosion performance of a range of commercial alumina-forming alloys is considered, some of the best performing alloys tend to contain more than one RE addition, e.g. General Electric Aircraft Engine's René N5, Haynes alloy 214 and Krupp VDM's Aluchrom YHf. Each alloy contains a

relatively low Y addition and either Hf and/or Zr. In Ni-base alloys, these "co-doped" alloys show improved scale adhesion and in Fe-base alloys, lower scale growth rates.[8]

In order to better understand the performance of co-doped alumina formers, commercially available and laboratory-made co-doped alloys have been tested in cyclic and isothermal oxidation tests at 1100°-1200°C and results have been compared to similar alloys with a single RE addition. Also, the alumina scales have been characterized after oxidation to determine the effect of co-doping on the scale microstructure. Of particular interest is that co-doping allows the RE addition to be minimized thereby reducing internal oxidation and the volume of RE-rich oxides within the scale. Using analytical transmission electron microscopy (TEM), the amount of Y, Hf and Zr ionic segregation on the alumina scale grain boundaries has been quantified. The results of this study indicate that co-doping allows the total RE addition to be minimized which produces optimized performance that cannot be obtained with a single RE addition. However, the RE and impurity levels need to be carefully controlled in order to obtain the co-doped benefits.

Experimental Procedure

The compositions of the alloys examined in this study are given in Table I in atom %, which is used throughout this paper. The commercial alloys were provided by the manufacturers. The laboratory-made alloys were inductively melted and cast in a chilled copper mold and annealed for 4h at 1300°C in a sealed quartz ampule prior to sectioning. Coupons ≈15mm in diameter and 1.0-1.5mm thick were cut and polished to a 0.3μm finish. All specimens were cleaned ultrasonically in acetone and methanol prior to oxidation. Oxidation exposures were conducted in resistively heated furnaces in either laboratory air or dry O_2 with temperatures of 1100°C for the Ni-base alloys and 1200°C for the Fe-base alloys. Isothermal reaction kinetics were measured using a Cahn model 1000 microbalance in dry flowing O_2. Mass changes were corrected for the evaporation of the Pt-Rh hangdown wire. Cyclic tests were conducted with cycle times at temperature of either 1h or 100h (more detailed experimental procedures are provided elsewhere[9]). Specimen mass gains were measured using a Mettler model AG245 balance.

After exposure, selected specimens were characterized by field emission gun (FEG), scanning

electron microscopy (SEM), electron probe microanalysis (EPMA), TEM and scanning transmission electron microscopy (STEM). Specimens were Cu-plated prior to sectioning for metallography. TEM cross-sectional specimens were prepared by the focused ion beam (FIB) technique.[10]

The TEM/STEM work was performed using a FEG Phillips CM200 equipped with an EmiSpec integrated acquisition system[11] for energy dispersive spectrometry (EDS) and electron energy loss spectroscopy (EELS). EDS spectrum images of the primary RE distributions (Hf, Y, Zr) along alumina grain boundaries were acquired in high resolution STEM mode with a nominal electron probe size of 1.0-1.2 nm. The EDS data were acquired using a spectrum image size of 200 nm x 200 nm, a pixel size of 2.0 nm, and a dwell time of 0.4 s. In this way, high resolution EDS maps were generated from several different grain boundaries in each specimen and at different locations within the scale (near the metal interface, near the center of the scale, and near the gas interface). The EDS maps were created by setting the window for each elemental peak at approximately full-width half-maximum and calculating the integrated intensity for the RE dopant peak (K_α or L_α) and Al(K_α). Thus, each pixel on the EDS map represented an integrated intensity for an individual element at that point. A series of line profiles was then extracted for the respective elements (using the same location on each set of maps) on each grain boundary map. An average RE/Al integrated intensity ratio as a function of distance across the grain boundary was determined from the series of line profiles generated for each sample and peak segregation values were determined from each average. The ratio is taken to correct for changes in TEM specimen thickness. Beam spreading likely is minimal in these analyses.[12]

Results

Oxidation performance and scale microstructure of Ni-base alloys

The first alloys to attract attention to the co-doping strategy were General Electric Aircraft Engine's René N5 and Haynes alloy 214 which strongly outperformed a variety of cast model NiCrAl bond coat alloys.[13] The excellent performance of these creep-resistant alloys compared to weaker compositions was contrary to the established model that better scale adhesion occurs on compliant substrates which are able to accommodate stresses from the scale.[14] However, the oxidation resistance

of these alloys was strongly temperature dependent, degrading rapidly at 1200°C, Table II, likely due to their relatively high coefficient of thermal expansion (CTE) compared to NiAl and FeCrAl.[13,16] Thus, their oxidation performance and scale microstructure were assessed at 1100°C where more extensive testing was performed.

Figure 1 shows the total and specimen mass gains of these alloys during 100h cycles at 1100°C. Both alloys showed some mass loss due to the spallation of the Ni-rich transient scale. However, the total mass gains for both alloys were low compared to FeCrAlY and approached the slow growth of Hf-doped NiAl which does not form a Ni-rich transient oxide.[17-20] René N5 and alloy 214 both showed excellent scale spallation resistance and slow scale growth with a minimal Y content (that would not typically result in good scale adhesion[13]), but was effective in conjunction with additions of Hf and/or Zr, Table I.

In order to further study this phenomenon, co-doped NiCrAl alloys with Hf and Y were made in the laboratory. Figure 2 shows results for a series of alloys with a base composition of Ni-20Cr-19Al. The co-doped alloy showed no mass loss or visual evidence of scale spallation until ≈800 1h cycles at 1100°C. Alloys with only Hf or Y additions showed significant scale spallation at much shorter times. Similar results were observed for base Ni-7Cr-13Al alloys.[8]

Characterization of the scales on the commercial alloys showed little or no internal oxidation. For example, after 100, 100h cycles at 1100°C, the scale formed on alloy 214 shows a relatively flat metal-scale interface and few RE-rich particles in or beneath the scale, Figure 3. Some Ni-rich scale remains at the gas interface but only in patches, as much of this outer layer has spalled.

In order to match an existing microstructural database,[19,21] the TEM cross-sections of the Ni-base alloys all were made after a standard exposure of 100, 1h cycles at 1100°C. (Previous work showed little difference between isothermal and cyclic exposures at this time and temperature.[19]) The scale formed on alloy 214 showed the anticipated duplex structure with an outer $Ni(Al.Cr)_2O_4$ layer and an inner, columnar α-Al_2O_3 scale, Figure 4. Despite the low levels of Y and Zr in this material, Table I, Y and Zr were still easily detected as segregants on the alumina scale grain boundaries in this specimen, Figure 5. A similar scale microstucture was observed to form on René N5, Figure 6. In this case, because of the Ta in the substrate, Ta-rich oxides (e.g. $NiTa_2O_6$) also were observed in the outer layer, especially at the

alumina-spinel interface (arrows in Figure 6).

For comparison, the scale formed on Y-doped Ni-20Cr-19Al is shown in Figure 7a. (The cyclic oxidation performance of this material is shown in Figure 2.) In this case, the spinel layer is thinner because this alloy contains more Al than either co-doped alloy, Table I, and numerous voids are observed at the spinel-alumina interface as has been observed for Ni_3Al.[22,23] Also, the columnar alumina grains are not as uniform and well-defined as for the scales formed on alloy 214 and René N5. However, the larger alumina grain diameters provide fewer diffusion paths for O diffusion. This TEM cross-section does not show the internal oxidation (i.e. oxide pegs) observed in the metallographic cross-section, which penetrated to ≈50μm in some locations.[19]

Figure 7b shows the alumina scale formed on co-doped Ni-20Cr-19Al containing Y and Hf. Compared to the scale formed on NiCrAlY, a similar spinel layer formed but the underlying alumina layer is thinner and has a smaller grain size. The oxide formed in the metal beneath the scale is due to internal oxidation which extended to a maximum depth of ≈10μm in some locations. The void in the center of the oxidized region is unusual. In general, the amount of internal oxidation for co-doped NiCrAl was less than for NiCrAlY but more than that observed for the commercial co-doped alloys. Thus the scales in Figure 7 show that co-doping reduced the inner alumina scale thickness but did not substantially change the grain structure.

Since single additions of Zr or Hf in NiCrAl did not significantly improve scale adhesion,[13] it was not possible to compare single-doped alumina scale microstructures after a similar exposure as the co-doped NiCrAl alloys. However, since single additions of these elements are effective in NiAl, Hf- and Zr-doped NiAl were examined to provide some information about the RE segregation behavior. Those scales are shown in Figure 8. Their scale microstructures are somewhat different because they do not form a Ni-rich transient scale but instead form cubic aluminas during their transient oxidation stage.[24,25] As was noted in a previous study,[19] the outer portion of the scale which transformed from the cubic θ phase to α-Al_2O_3 contains more voids in both cases. The inner portion of the scale which formed as α-Al_2O_3 is more dense and defect free. Compared to the inner alumina scales formed on the NiCrAl alloys, the scale also is thinner and typically only one grain thick.

Oxidation performance and scale microstructure of Fe-base alloys

A similar co-doping strategy can be used with Fe-base alloys. In this case, because of their better scale adhesion and existing microstructural database, the Fe-base alloys were tested at 1200°C, Table II. A series of co-doped Fe-20Cr-10Al alloys was fabricated with different Y and Hf contents,[8] Table I. Figure 9 shows the slower isothermal scale growth rate achieved by co-doping with a low total RE content. The oxidation rate for the slowest growing scale on co-doped FeCrAl approaches that for Hf-doped Fe_3Al,[26] Table II. In long-term cyclic testing using 100h cycles, the potential benefit of co-doping was more clearly observed, Figure 10. The co-doped FeCrAl showed more scale spallation than FeCrAlY, but a significantly lower total mass gain because of its slower scale growth rate. However, because of the long life of FeCrAlY at 1200°C, (≈9000, 1h cycles normalized to a 1.5mm thick specimen[7-9]) it has not been determined yet if co-doped FeCrAl alloys can exceed the oxidation-limited lifetime of FeCrAlY.[8]

Characterizing the scale formed on FeCrAlY and the three co-doped alloys after 10, 100h cycles at 1200°C showed some interesting trends. The most significant effect of co-doping was on the scale thickness and amount of internal oxidation, Figure 11. Obviously, the alloy with 0.14%Hf and Y was significantly overdoped and massive internal oxidation occurred, Figure 11b. (It is worth noting that several early studies of the RE effect used alloys with similar dopant concentrations to reach the incorrect conclusion that RE additions do not reduce the growth rate of alumina scales.) As the RE content was reduced in the other co-doped alloys, the depth and volume of internal oxidation was greatly reduced compared to FeCrAlY, Figure 11.

In addition to the reduction in internal oxidation, minimizing the RE content in the alloy also reduced the volume of RE-rich particles in the alumina scale. Figure 12 focuses on the scale portion of the cross-sections shown in Figure 11 using SEM back-scattered electron imaging. From this series of micrographs it is clear that the volume of RE-rich particles is still significant in the scale formed on FeCrAl+0.02%Hf,Y but is greatly reduced compared to the other alloys. Since RE-rich oxides are generally fast oxygen conductors, it is obvious that minimizing the volume of RE-rich particles in the scale should reduce the scale growth rate.[27]

Again, to utilize an existing microstructural database,[6,19,20,26] all of the TEM cross-sections were made after 2h at 1200°C. Figure 13a shows the scale formed on FeCrAlY which is not unlike those formed on the Ni-base alloys at 1100°C. The smaller, outermost grains at the gas interface are α-Al_2O_3 but contain higher quantities of Fe and Cr than the columnar grains. A similar grain structure developed on Hf-doped Fe_3Al.[26] The image in Figure 13b of the alumina scale formed on FeCrAl+0.02%Hf,Y is somewhat difficult to interpret because the grain structure is less well defined than in Figure 13a due to magnetic distortion. In this case, the low level of RE dopant in the co-doped alloy may have had a limited effect on the scale microstructure at this relatively early stage of oxidation and there is no significant difference in scale thickness at this point. A similar observation was made for low levels of Zr in FeCrAl.[28] However, RE-rich particles had already formed within the scale at this stage (bright grains in Figure13b). While a clear columnar grain structure is not as evident, the grain size generally is similar to that observed in the scale formed on FeCrAlY.

Quantification of Segregation

The ionic segregation of RE additions to alumina scale grain boundaries has been widely observed for a variety of RE dopants and at various oxidation times and temperatures. These findings in the literature have been summarized several times.[6,7,29] Thus, it is not surprising that each of the alloys studied here showed grain boundary segregation of each of the dopants present in the substrate, e.g. Figure 5. A more interesting goal is to quantify and compare the relative amounts of segregation observed in each case and, particularly, to compare the amount of segregation observed in the single-doped alloys to that in the co-doped alloys. Some initial results quantifying the amount of grain boundary segregation (reported as RE/Al ratios) observed in the scales of these specimens is shown in Table III. The results are the average peak intensity ratios, and are listed by location in the scale because of observations that the amount of segregation is not constant across the scale.[23]

Figure 14a gives an example of the profiles obtained in the alumina scale near the metal-scale interface in the Fe-base alloys. The amount of Hf on the scale boundary formed on Hf-doped Fe_3Al is significantly higher than the Y measured in the scale formed on FeCrAlY or the Hf or Y measured in the scale formed on FeCrAl+0.02%Hf,Y. Figure 14b shows the peak segregation values plotted as a function

of location in the scale for several of the Ni-base alloys. A previous study of the Y and Zr segregation in the scale formed on Y_2O_3-dispersed Ni_3Al after 40h at 1200°C showed the amount of segregation decreased from the gas interface towards the metal interface.[23] However, the results in Figure 14b measured in scales formed at 1100°C show no consistent trend.

For comparison with the segregation observed in the scales formed on single-doped and co-doped alloys, Figure 15a shows the average peak segregation values plotted versus the concentration of the segregating element in the substrate for the Fe-base alloys oxidized for 2h at 1200°C and Ni-base alloys oxidized for 100h at 1100°C. There is a general upward trend but several exceptions are noted. Also, the amount of segregation does not strongly increase with RE content. For example, increasing the amount of Zr in the Ni-base alloys by a factor of 4 only increased the amount of segregation by a factor of 2. Several studies have suggested that the ratio of the dopants to other impurities, especially C and S, has a strong affect on efficacy of the dopant.[7,30-34] To explore this relationship, the segregation values also were plotted in Figure 15b versus the Y/S, Hf/C or Zr/C ratios found in Table I. This produced a similar level of consistency as in Figure 15a.

Another way of considering the segregation results is as a function of their effectiveness, e.g. the change in the scale growth rate, Table II. Figure 16a shows the sum of the peak segregation values measured in the scale near the substrate in each of the Ni-base alloys, plotted versus the steady-state parabolic rate constant at 1100°C. Figure 16b plots the results for the Fe-base alloys at 1200°C. In both cases, there is a general trend towards lower rates with more segregation for the single-doped alloys but the co-doped alloys do not follow a similar pattern. The co-doped alloys exhibited relatively low rate constants but, in most cases, have relatively low levels of segregation. In general, the Hf-doped aluminides consistently show the highest levels of segregation intensity ratios and the lowest scale growth rates. However, while this type of analysis readily allows comparison of segregation levels for a given element between different materials, when comparing the values for different elements, more work is needed to verify the quantification technique.

Figure 17 may show one implication of the lower grain boundary segregation in scales formed on co-doped alloys. These are the same alumina scales shown in Figure 11. This series shows that the grain

size of the alumina scale at the gas interface decreased with decreasing RE content. This may appear counter-intuitive as RE-doping at grain boundaries is expected to refine the grain size,[6] as it does in bulk alumina.[35] However, these results can be explained in terms of the dynamic model where RE ions in a growing scale are diffusing towards the gas interface,[6] and as these ions supersaturate on the grain boundaries at the gas interface over time,[29] they nucleate to form RE-rich oxide particles at the gas interface (bright particles in Figure 11). With high RE contents in the alloy and more RE ions diffusing to the gas interface, the result is more RE-rich oxide nucleation and growth and lower "steady-state" ionic segregation on the grain boundaries.[29] As discrete oxide particles, rather than grain boundary segregants, the RE dopant is ineffective in reducing the growth of the alumina grains at the gas interface. However, with the lowest RE contents in the 0.02%Hf,Yco-doped alloy, a lower RE ion flux on the grain boundaries requires longer times to reach supersaturation and thus higher concentrations of RE ions remain on the scale grain boundaries to inhibit grain growth. A finer scale grain size, with more diffusion pathways, is not necessarily a benefit, however, it is clearly an effect of reducing the RE content of the alloy.

Discussion

The goal of this work was to gain a better understanding of why co-doping is an effective strategy for optimizing the RE effect in alumina-forming alloys. Based on these results it appears that the reason co-doping is effective is that it allows the total RE content to be reduced while still maintaining the RE benefits such as good scale adhesion and low scale growth rates. TEM cross-sections did not show any significant change in the scale microstructure with co-doping and analysis of the grain boundary segregation did not reveal any significant increase or decrease in the amount of segregation when more than one RE was added to the substrate.

The clear difference between the single-doped and co-doped alloys was the reduction in the amount of internal oxidation in the alloy and a lower concentration of RE-rich oxides within the alumina scale. Early work on RE effects noted that Y-rich internal oxides appeared to be associated with scale spallation[36] and more recent work on Y doping in NiCrAl alloys observed a similar effect.[13,37] It also

has been noted previously that RE-rich oxides contribute to faster scale growth because they allow faster bulk O diffusion than alumina[27] or by providing heterogeneous interfaces within the scale where O diffusion rates may be faster.[38] In numerous studies, an optimum RE level was attained where the beneficial effects were maximized, e.g. where the parabolic rate constant was minimized.[1,7,8] At lower than optimum dopant levels, little or no RE effect was observed, presumably because there was insufficient dopant and, at higher concentrations, the oxidation rate began to increase as "over-doping" problems, such as internal oxidation, became detrimental. One issue for Y is that it has a relatively low solubility limit in both Ni- and Fe-base alloys, such that at the optimum Y content for NiCrAl, internal oxidation was still evident.[37] By lowering the Y content, less internal oxidation occurred but the RE benefits, especially spallation resistance, began to degrade.[13] Thus, one obvious advantage of co-doping is that the Y content can be lowered (Table I) to below the optimal level needed for a single Y-doped alloy. This reduces any potential detrimental effects.

These observations for Y might suggest that other RE dopants would be more effective. However, the co-doped performance was not achieved without the small Y addition,[8] e.g. Figure 2. It has been suggested that a Y/S ratio > 1 is needed to getter excess S in the alloy and prevent the detrimental effects associated with S.[30,31,34] Such a critical ratio was observed in these co-doped alloys, as shown in Table I. In addition, a commercial co-doped FeCrAl, Aluchrom HF, contains an even lower S level than in these laboratory-made FeCrAl alloys.[39] During development of the co-doped laboratory alloys, when the Y/S ratio was less than one, poor scale adhesion was observed.[8] However, these observations do not elucidate any mechanistic significance of this ratio. Scale adhesion was not a problem for Hf- and Zr-doped NiAl because of their low S contents, Table I. In Hf-doped NiAl, the Hf/C ratio has been observed to be important in optimizing scale adhesion.[33] However, that ratio or the Zr/C ratio has not been proven to be critical for co-doped alloys, Table I.

The grain boundary segregation quantification work was undertaken to determine if the use of two or more dopants increased the total amount of segregation by some synergistic effect. It also is possible that dopants of different sizes or charges segregate to different sites on the alumina grain boundaries, resulting in a stronger influence on diffusion in the scale. While the latter hypothesis is still

a possibility, the former does not appear to occur. The amount of segregation detected in the scales on the co-doped alloys was not higher than in the single-doped alloys. There was some correlation between the alloy RE content and the amount of segregation detected, Figure 14a, but no consistent relationship was observed. With low levels of Y in the co-doped alloys, Y ions were detected on the scale grain boundaries suggesting that 20-30ppma was sufficient to create the beneficial effects[6] and higher Y contents only increase the number of Y-rich oxides in the alloy and within the oxide. This observation is consistent with results for René N5 where Y contents between ~10-100ppma produced similar improvements in scale adhesion.[34] Furthermore, the excellent performance of alloy 214 suggests that the second element (Zr for alloy 214) also is only needed at a low level. Higher quantities of Zr or Hf leads to increased RE-rich oxide formation, Figure 12. Thus, the current lowest RE content in co-doped FeCrAl might be further reduced. This could result in even fewer RE-rich particles in the scale, Figure 13d, and potentially lower scale growth rates.

In developing an optimized alumina-forming alloy, several areas have already been widely addressed in the literature, such as CTE mismatch between alloy and scale, S impurity management and stress relaxation in the substrate. The CTE issue is clear in the divergent performance of the various NiCrAl and FeCrAl alloys between 1100° and 1200°C, Table II. NiCrAl-based alloys with a larger CTE mismatch with alumina than FeCrAl-based alloys are expected to have more spallation problems as the temperature increases. Sulfur effects have been mentioned above, and low levels of Y appear to mitigate any detrimental sulfur effect. The ability of the substrate to relieve stress in the scale[14] is an important issue especially for FeCrAl where wrought alloys are the most spallation-resistant, but have low creep strength. Oxide dispersion strengthened FeCrAl alloys have much better creep strength but also suffer more scale spallation.[7,9,40] If corrosion-resistant structural alloys are required, some compromise is necessary. Weaker materials may be used in non-structural applications or as coatings. The type and amount of RE dopant is one area with further potential for optimization. As mentioned previously, single dopant optimization studies have been widely reported, but co-doping opens the possibility for future improvements.

Summary

The oxidation performance of Ni- and Fe-based co-doped alumina-forming alloys show improved scale adhesion and/or slower scale growth rates compared to similar alloys with single RE additions. The addition of two or more dopants does not appear to result in any significant change in the scale microstructure or the amount of ionic segregation on the alumina scale grain boundaries. Co-doping does allow for lower total amounts of RE dopant in the alloy which reduces the amount of internal oxidation and the volume of RE-rich oxides within the scale. These changes appear to result in improved oxidation performance suggesting that co-doping strategies in alumina-forming alloys will produce an optimized RE effect in terms of scale adhesion and slow scale growth, and likely improve the oxidation-limited life of alloys and coatings. These results also suggest that RE dopants are effective when located on the scale grain boundaries as ions, but when they form RE-rich oxides beneath or within the scale they detract from the beneficial RE effect.

Acknowledgments

The authors would like to thank G. Garner, L. D. Chitwood, K. S. Trent, T. Brummitt, D. Coffey and H. Longmire at ORNL for assistance with the experimental work and D. F. Wilson and P. F. Tortorelli at ORNL for their comments on the manuscript. The alloys were provided by M. Harper, Haynes (alloy 214) and S. Walston, GEAE (René N5). This research was sponsored by the U.S. Department of Energy, Office of Fossil Energy, Advanced Research Materials Program and the Office of Power Technology, Distributed Energy Resources Program under contract DE-AC05-00OR22725 with UT-Battelle, LLC.

References

1. Whittle, D. P. and Stringer, J., Improvement in properties: Additives in oxidation resistance. *Philos. Trans. R. Soc. London*, A, **295**, 309-29 (1980).
2. Lang, E. (Ed.), *The Role of Active Elements in the Oxidation Behavior of High Temperature Metals and Alloys*. Elsevier Applied Science, London, U.K., 1989.
3. King, W. E. (Ed.), Mater. Sci. Forum, Vol. 43, *The Reactive Element Effect on High Temperature*

Oxidation -- After Fifty Years. Trans Tech Publications, Winterthur, Switzerland, 1989.

4. Moon, D. P. Role of reactive elements in alloy protection. *Mater. Sci. Technol.*, **5**, 754-64 (1989).
5. Strawbridge, A. and Hou, P.Y. The role of reactive elements in oxide scale adhesion. *Mater. High Temp.*, **12**, 177-81 (1994).
6. Pint, B. A. Experimental observations in support of the dynamic segregation theory to explain the reactive element effect. *Oxid. Met.*, **45**, 1-37 (1996).
7. Pint, B. A. Progress in understanding the reactive element effect since the Whittle and Stringer literature review. in Proceedings of the John Stringer Symposium. Edited by P. F. Tortorelli and P. Y. Hou. ASM, Materials Park, OH, in press.
8. Pint, B. A. Optimization of reactive element additions to improve oxidation performance of alumina-forming alloys. submitted to J. Am. Ceram. Soc. (2002).
9. Pint, B. A., Tortorelli, P. F., and Wright, I. G., Effect of cycle frequency on high temperature oxidation behavior of alumina-forming alloys. *Oxid. Met.*, **58**, 73-101 (2002).
10. More, K. L., Coffey, D. W., Pint, B. A., Trent, K. S. and Tortorelli, P. F. TEM specimen preparation of oxidized Ni-based alloys using the focused ion beam (FIB) technique. (Paper presented at Microscopy and Microanalysis 2000, Philadelphia, PA, August 2000).
11. www.EmiSpec.com
12. Furdanowicz, W., Garratt-Reed, A. J. and Vander Sande, J. B. Measurements of beam-broadening in samples observed with a FEG-STEM. Inst. Phys. Conf. Ser. No. 119: Sec. 10, 437-441 (1991).
13. Pint, B. A. and Wright, I. G., Cyclic oxidation behavior of cast NiCrAl alloys. In: *High Temperature Corrosion and Materials Chemistry*. Proc. Vol.98-9 (Eds. P. Y. Hou, M. J. McNallan, R. Oltra, E. J. Opila and D. A. Shores) Electrochem. Soc., Pennington, NJ, pp.263-74 (1998).
14. Evans, H. E., Nicholls, J. R. and Saunders, S. R. J., The influence of diffusion-related mechanisms in limiting oxide-scale failure. *Solid State Phenom.*, **41**, 137-56 (1995).
15. Wright, I. G., Pint, B. A., Hall, L. M. and Tortorelli, P. F. Experimental results and modeling related to oxidation lifetimes. In: *Lifetime Modelling of High Temperature Corrosion Processes*. (Eds. M. Schütze, W. J. Quadakkers and J. R. Nicholls) Maney, London, pp.339-58 (2001).
16. Haynes, J. A., Pint, B. A., Porter, W. D. and Wright, I. G. Relationships between thermal expansion and oxidation behavior of various superalloys and high-temperature coating materials. for submission to *Mater. High Temp.* (2002).
17. Doychak, J., Unpublished research, NASA Lewis Research Center, Cleveland, OH, 1994.
18. Pint, B. A., Wright, I. G., Lee, W. Y., Zhang, Y., Prüßner, K. and Alexander, K. B. Substrate and bond coat compositions: Factors affecting alumina scale adhesion. *Mater. Sci. Eng.*, **A245**, 201-211 (1998).
19. Pint, B. A., More, K. L., Wright, I. G. and Tortorelli, P. F., Characterization of thermally cycled alumina scales. *Mater. High Temp.*, **17**, 165-71 (2000).

20. Pint, B. A., More, K. L. and Wright, I. G. The effect of quaternary additions on the oxidation behavior of Hf-doped NiAl. *Oxid. Met.*, in press (2003).
21. Pint, B. A., More, K. L. and Tortorelli, P. F., The effect of water vapor on oxidation performance of alloys used in recuperators. ASME Paper #2002-GT-30543, presented at the International Gas Turbine & Aeroengine Congress & Exhibition, Amsterdam, Netherlands, June 3-6, 2002.
22. Doychak, J. and Rühle, M. TEM studies of oxidized NiAl and Ni_3Al cross sections. *Oxid. Met.*, **31**, 431-52 (1989).
23. Pint, B. A., Garratt-Reed, A. J. and Hobbs, L. W., Analytical electron microscopy study of the breakdown of α-Al_2O_3 scales formed on oxide dispersion strengthened alloys. *Oxid. Met.*, **56**, 121-47 (2001).
24. Hagel, W. C. The oxidation of iron, nickel and cobalt-base alloys containing aluminum. *Corr.*, **21**, 316-26 (1965).
25. Rybicki, G. C. and Smialek, J. L. Effect of the θ - α-Al_2O_3 transformation on the oxidation behavior of β-NiAl+Zr. *Oxid. Met.*, **31**, 275-304 (1989).
26. Pint, B. A., More, K. L., Tortorelli, P. F., Porter, W. D. and Wright, I. G., Optimizing the imperfect oxidation performance of iron aluminides. *Mater. Sci. Forum*, **369-372**, 411-8 (2001).
27. Hindam, H. and Whittle, D. P. Peg formation by short-circuit diffusion in Al_2O_3 scales containing oxide dispersions," *J. Electrochem. Soc.*, **129**, 1147-9 (1982).
28. Pint, B. A., Garratt-Reed, A. J. and Hobbs, L. W. The reactive element effect in commercial ODS FeCrAl alloys. *Mater. High Temp.*, **13**, 3-16 (1995).
29. Pint, B. A., Garratt-Reed, A. J. and Hobbs, L. W. Possible role of the oxygen potential gradient in enhancing the diffusion of foreign ions on α-Al_2O_3 grain boundaries. *J. Am. Ceram. Soc.*, **81**, 305-14 (1998).
30. Sigler, D. R. Aluminum oxide adherence on Fe-Cr-Al alloys modified with group IIIB, IVB, VB, and VIB elements. Oxid. Met., 32 337-55 (1989).
31. Smialek, J. L., Jayne, D. T., Schaeffer, J. C. and Murphy W. H. Effects of hydrogen annealing, sulfur segregation and diffusion on the cyclic oxidation resistance of superalloys: A review. *Thin Solid Films*, **253**, 285-92 (1994).
32. Sarioglu, C., Stinner, C., Blachere, J. R., Birks, N., Pettit, F. S. and Meier, G. H. The control of sulfur content in nickel-base single crystal superalloys and its effects on cyclic oxidation resistance. In: *Superalloys 1996*. (Eds. R. D. Kissinger, D. J. Deye, D. L. Anton, A. D. Cetel, M. V. Nathal, T. M. Pollack, D. A. Woodford) TMS, Warrendale, PA, pp.71-80 (1996).
33. Wright, I. G. and Pint, B. A. Some effects of interactions among minor element additions on the high-temperature oxidation behavior of Ni-base alumina-forming alloys. In: *Proc. SF2M 2000*, Journées d'automne, Société Française de Métallurgie et de Matériaux, Paris, pp.86-87 (2000).
34. Smialek, J. L. and Pint, B. A. Optimizing scale adhesion for single crystal superalloys. *Mater.*

Sci. Forum, **369-372**, 459-66 (2001).

35. Fang, J., Thompson, A. M., Harmer, M. P. and Chan, H. M. Effect of Y and La on the sintering behavior of ultra-high purity Al_2O_3. *J. Am. Ceram. Soc.*, **80**, 2005-12 (1997).
36. Kuenzly, J. D. and Douglass, D. L. The oxidation mechanism of Ni_3Al containing yttrium. *Oxid. Met.*, **8**, 139-178 (1974).
37. Prüßner, K. and Alexander, K. B. Unpublished research, Oak Ridge National Laboratory, Oak Ridge, TN, 1998.
38. Tortorelli, P. F., DeVan, J. H., McKamey, C. G. and Howell, M. Influence of oxide reinforcements on high-temperature oxidation resistance of Ni_3Al matrix composites. *Ceram. Trans.*, **19**, 961-8(1991).
39. Quadakkers, W. J., Nicholls, J., Naumenko, D., Wilber, J. and Singheiser, L. Factors affecting oxide growth rates and lifetime of FeCrAl alloys. In: *Materials Aspects in Automotive Catalytic Converters*. (Ed. H. Bode) Wiley-VCH, Weinheim, Germany, pp.93-105 (2002).
40. Wilber, J. P., Bennett, M. J. and Nicholls, J. R., Life-time extension of alumina forming FeCrAl-RE alloys: Influence of alloy thickness. *Mater. High Temp.*, **17**, 125-32 (2000).

Table I. Chemical composition (in atomic%) of alloys examined in this study obtained by inductively coupled plasma analysis and combustion analysis. Composition ratios of interest also have been calculated.

Alloys:	NiAl	NiAl	NiCrAl	René N5	Alloy 214	NiCrAl	FCAY	Fe_3Al	FeCrAl	FeCrAl	FeCrAl
Dopant(s):	Hf	Zr	Y	Hf,Y,Zr	Zr,Y	Hf,Y	Y	Hf	Hf,Y	Hf,Y	Hf,Y
Ni	49.83	49.95	60.92	64.85	70.54	61.37	<0.01	<0.01	<0.01	0.01	0.01
Fe	<0.01	<0.01	<0.01	0.08	3.37	0.01	69.83	69.58	69.58	70.08	69.58
Cr	0.01	<0.01	19.95	7.79	16.73	19.54	20.21	1.98	20.32	20.07	20.28
Al	50.07	49.99	19.01	13.88	8.73	18.94	9.86	28.09	9.90	9.79	10.09
Si	<0.01	<0.01	<0.01	0.15	0.16	0.02	<0.01	<0.01	<0.01	<0.01	<0.01
Ti	<0.01	<0.01	<0.01	0.013	0.01	<0.01	<0.01	<0.01	<0.01	<0.01	<0.01
Y	<0.01	<0.01	**0.052**	**0.003**	**0.0025**	**0.006**	**0.082**	<0.01	**0.094**	**0.003**	**0.002**
Zr	<0.01	**0.052**	<0.01	**0.003**	**0.0120**	<0.01	<0.01	<0.01	<0.01	<0.01	<0.01
Hf	**0.048**	<0.01	<0.01	**0.054**	<0.01	**0.046**	<0.01	**0.053**	**0.047**	**0.035**	**0.018**
Other			0.01 Cu	2.11 Ta 1.61 W 1.02 Re 7.28 Co 0.90 Mo	0.17 Mn 0.02 Co 0.01 Mo	0.02 Cu	0.01 Cu				
B	<0.001	0.003	<0.001	0.028	0.005	0.005	<0.001	0.004	<0.001	0.005	0.005
P	<0.005	<0.005	<0.005	0.004	0.007	<0.005	<0.01	<0.005	<0.005	<0.005	0.005
C	0.036	<0.04	0.043	0.249	0.225	0.042	<0.04	0.040	0.040	<0.04	0.010
N (ppma)	<4	<4	15	<4	101	37	11	<4	11	<10	15
O (ppma)	43	48	58	52	48	109	110	66	85	69	39
S (ppma)	<4	4	8	7	5	5	16	31	15	16	16
Y/S			65	4	5	12	51		63	2	2
Hf/C	1.3			0.2		1.1		1.3	1.2	≈1	1.8
Zr/C		1.3		0.01	0.05						

Table II. Isothermal parabolic rate constants and specimen and total mass changes for various cyclic exposures at 1100° and 1200°C for the alloys in this study.

Temperature:	1100°C					1200°C				
Conditions:	Isotherm.	100x1h	1000x1h	20x100h	20x100h	Isotherm.	100x1h	1000x1h	10x100h	10x100h
Mass Change:	rate	spec.	spec.	total	spec.	rate	spec.	spec.	total	spec.
Units	g^2/cm^4s	mg/cm^2	mg/cm^2	mg/cm^2	mg/cm^2	g^2/cm^4s	mg/cm^2	mg/cm^2	mg/cm^2	mg/cm^2
NiAl+Hf	$0.53x10^{-13}$	0.29	0.42	0.85	0.76	$0.8x10^{-12}$	0.54	0.89	1.94	0.42
NiAl+Zr	10	0.38	1.01	not tested		3.6	0.67	1.14	2.90	1.63
NiCrAlY	14	0.51	-5.03	8.84	-9.19	7.8	-5.84	-8.92[b]	13.42	-5.28
René N5	1.2	0.35	0.61[a]	1.39	0.97	1.2	0.14	-2.42[c]	3.08	-2.41
Alloy 214	0.8	-0.04	-0.29	1.26	0.62	0.8	0.56	-41.33	2.37	0.81
NiCrAl+Y,Hf	3.6	0.43	0.77	2.00	0.58	2.6	0.83	-4.28	4.68	-2.46
FeCrAl+Y	4.3	0.55	1.31	2.81	2.74	7.5	1.50	1.63	3.71	3.68
Fe_3Al+Hf	3.7	0.60	1.68	1.93	1.58	1.4	0.78	0.09	2.85	1.06
FeCrAl+0.14Y,Hf	18	not tested		4.43	4.29	33	3.42	8.09	9.05	8.85
FeCrAl+0.04Y,Hf	2.0	0.71	1.62	2.27	2.22	5.6	1.32	2.04	2.96	2.85
FeCrAl+0.02Y,Hf	1.2	0.49	1.12	1.33	1.30	3.5	0.84	1.34	1.82	1.73

a 926 cycles at 1100°C
b 250 cycles at 1200°C
c 500 cycles at 1200°C

Table III. STEM/EDX alumina grain boundary segregation data showing the peak x-ray intensity ratios (RE/Al) and standard deviations as a function of location within the scale: at the metal-scale interface (int), in the middle of the scale (mid) and at the gas interface (gas).

Alloys:	NiAl	NiAl	NiCrAl	René N5	Alloy 214	NiCrAl	FeCrAlY	Fe_3Al	FeCrAl
Dopant(s):	Hf	Zr	Y	Hf,Y,Zr	Zr,Y	Hf,Y	Y	Hf	Hf,Y
Hf int	0.046±0.009			0.026±0.006		0.021±0.005		0.032±0.01	0.014±0.003
Hf mid	0.037±0.009								
Hf gas	0.023±0.008								
Y int			0.013±0.003	0.004±0.002	0.011±0.003	0.007±0.002	0.018±0.005		0.004±0.001
Y mid			0.015±0.004		0.007				
Y gas			0.017±0.005		0.010				
Zr int		0.019±0.006		0.006±0.002	0.009±0.002				
Zr mid		0.022±0.007			0.006				
Zr gas		0.015±0.004			0.007				

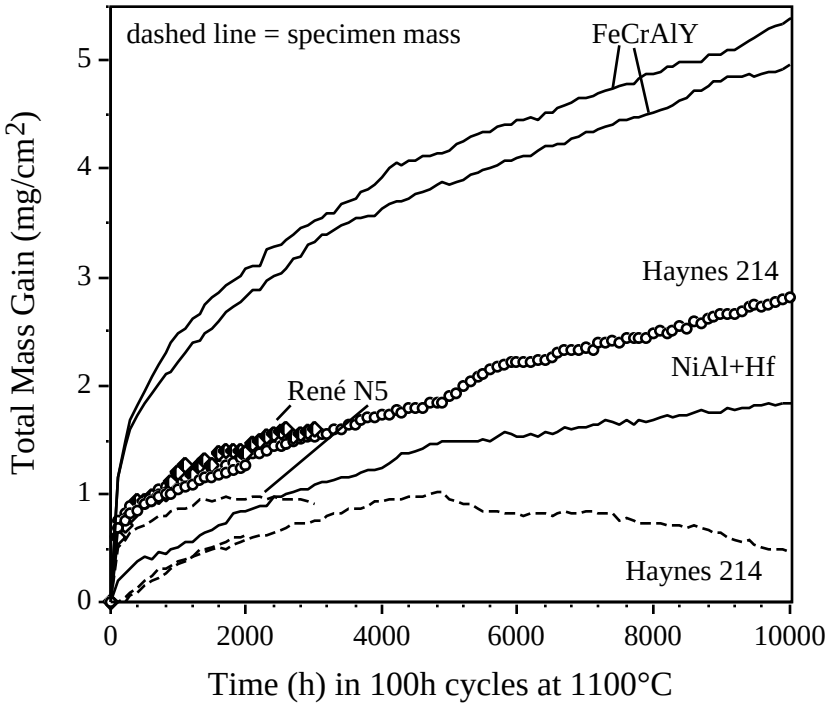

Figure 1. Total and specimen mass gains for several materials tested in 100h cycles at 1100°C. Haynes 214 and René N5 both show scale spallation but relatively low mass gains relative to FeCrAlY.

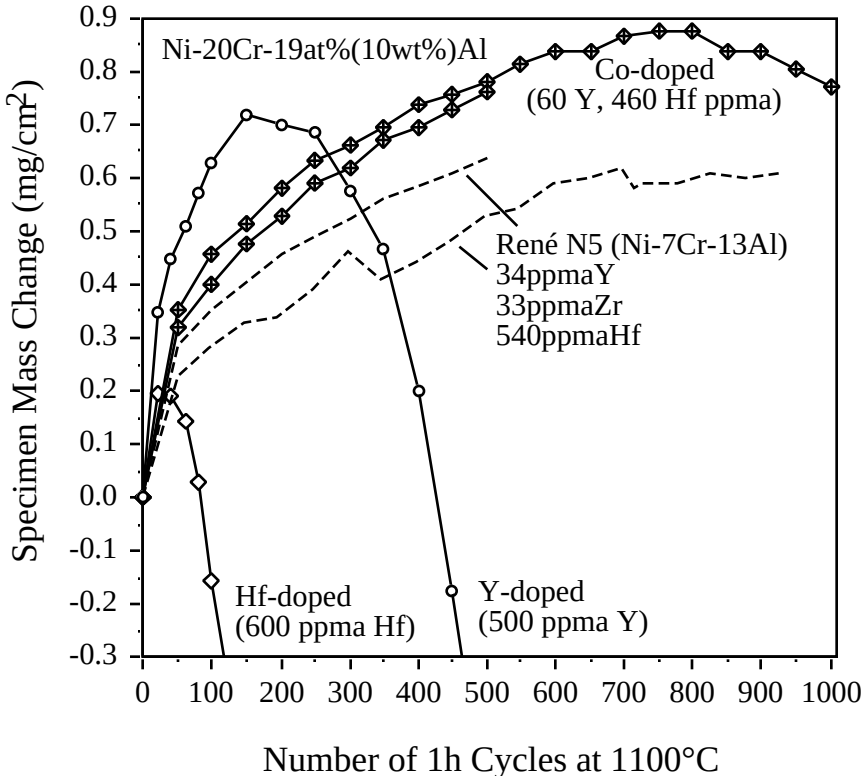

Figure 2. Specimen mass change during testing in 1h cycles at 1100°C for various NiCrAl alloys.

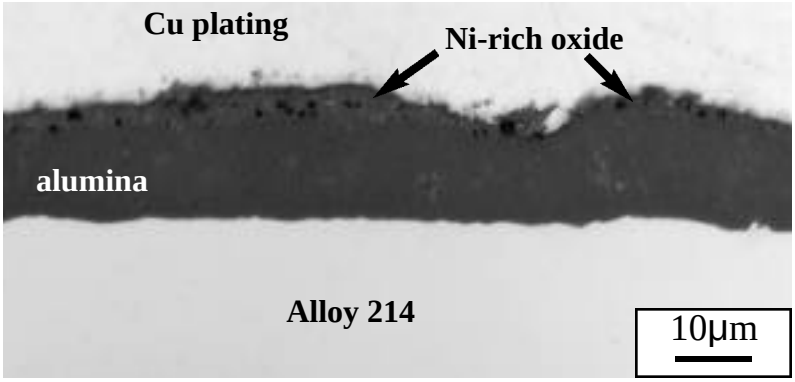

Figure 3. Polished cross-section of the duplex scale remaining on Haynes 214 after 100, 100h cycles at 1100°C.

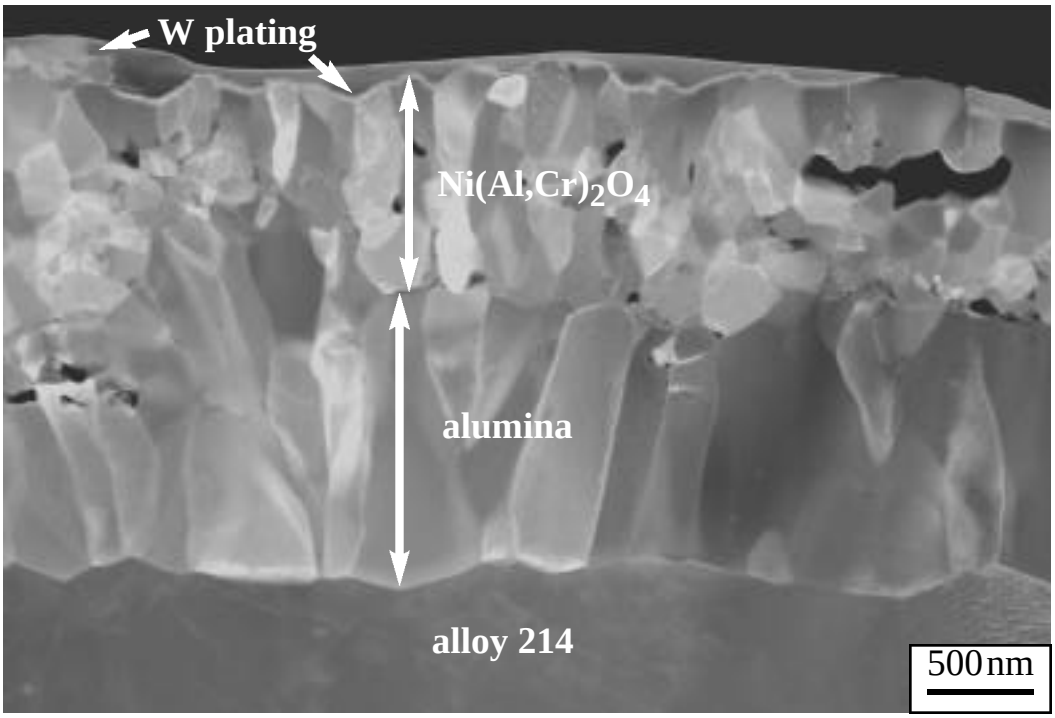

Figure 4. STEM annular dark field image of the duplex scale formed on alloy 214 after 100, 1h cycles at 1100°C. An inner columnar alumina layer and an outer spinel layer were observed.

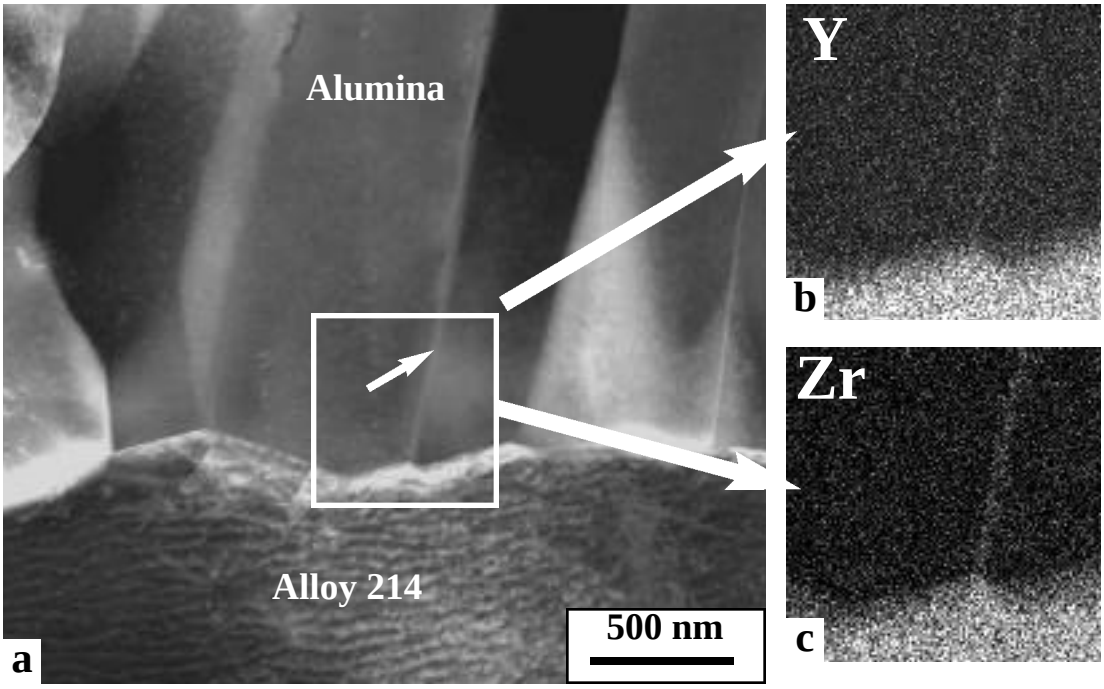

Figure 5. (a) STEM annular dark field image of the duplex scale formed on alloy 214 after 100, 1h cycles at 1100°C. (b) Y x-ray map and (c) Zr x-ray map from the box in (a) showing segregation of both elements.

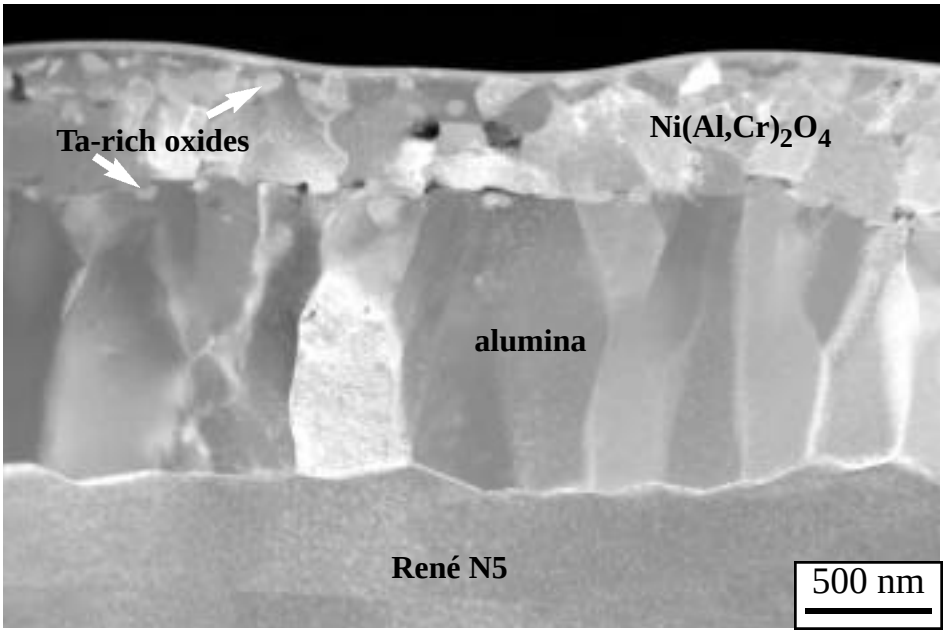

Figure 6. STEM annular dark field image of the duplex scale formed on alloy 214 after 100, 1h cycles at 1100°C.

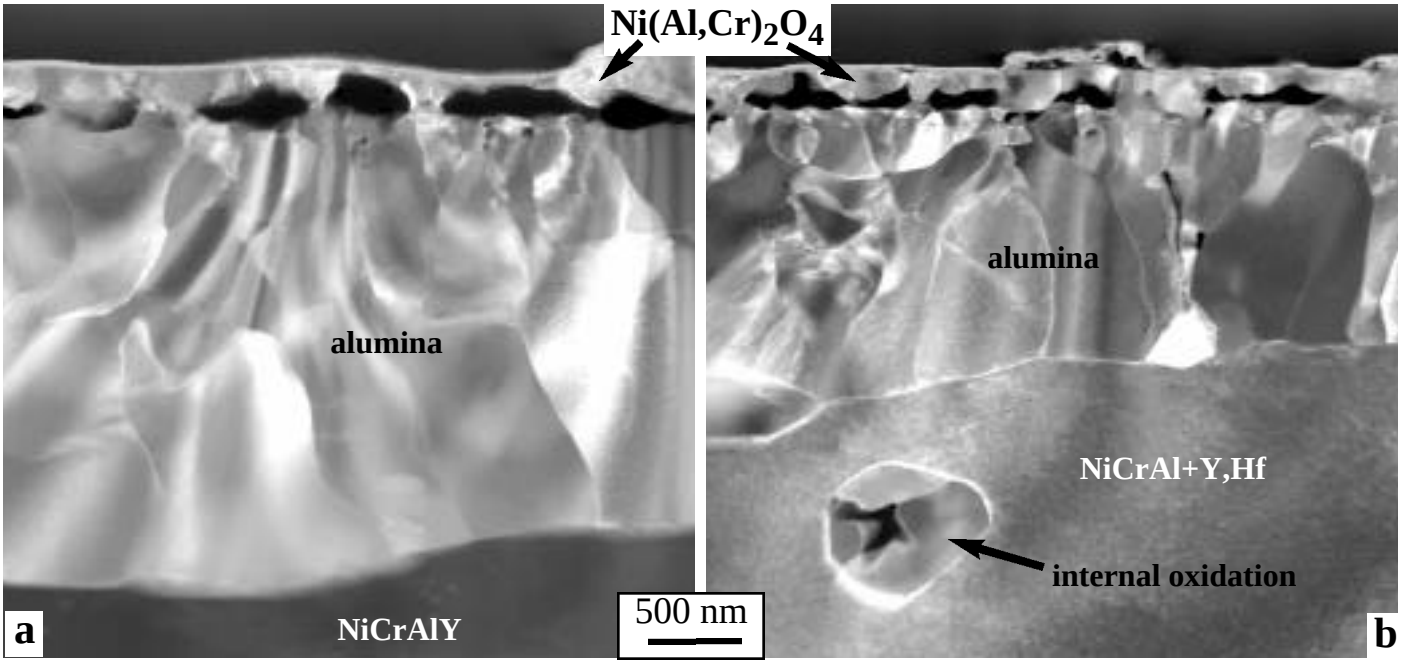

Figure 7. STEM annular dark field images of the duplex scales formed after 100, 1h cycles at 1100°C formed on (a) NiCrAlY and (b) NiCrAl doped with Y and Hf.

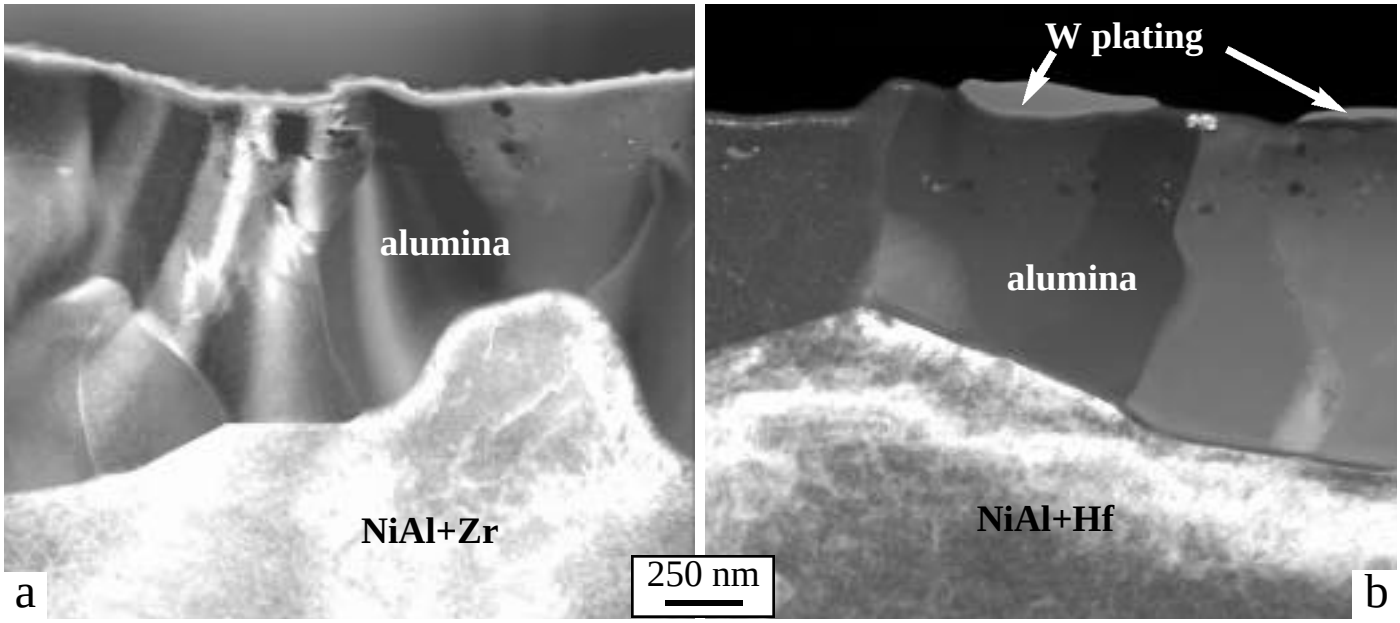

Figure 8. TEM cross-sections of the scale formed after 100, 1h cycles at 1100°C on (a) NiAl+Zr and (b) NiAl+Hf.

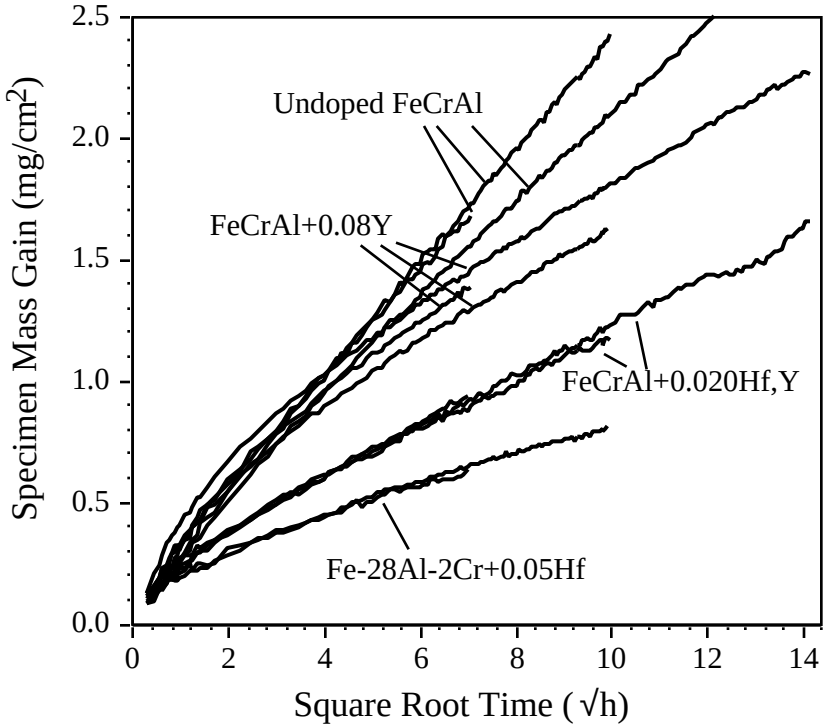

Figure 9. Isothermal mass gain data at 1200°C plotted versus the square root of time for various Fe-base alloys.

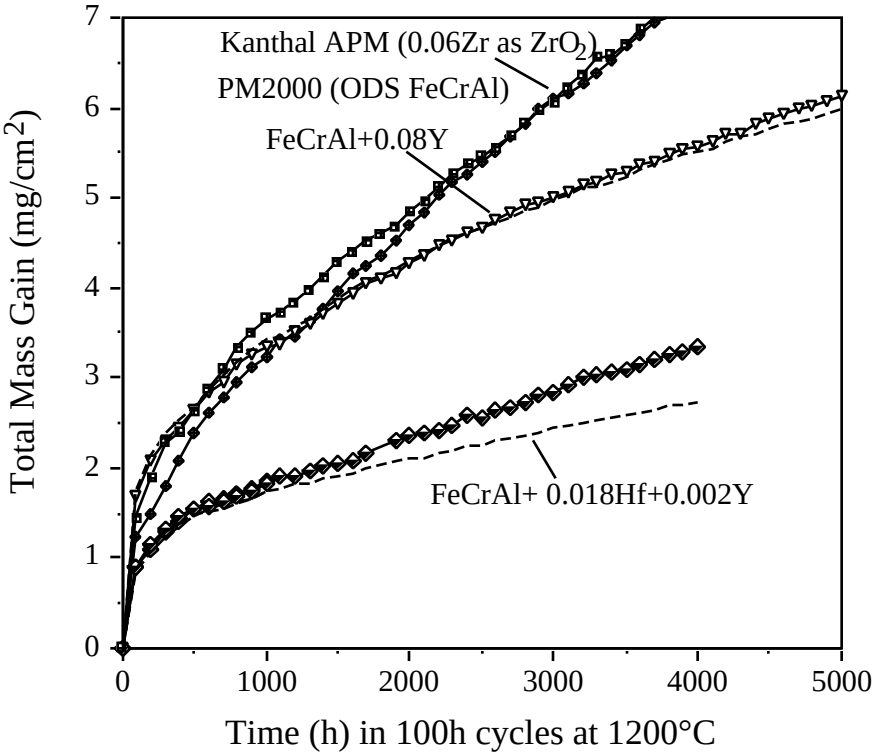

Figure 10. Total mass gain (symbols) and specimen mass change (dashed lines) during 100h cycles at 1200°C for various FeCrAl alloys.

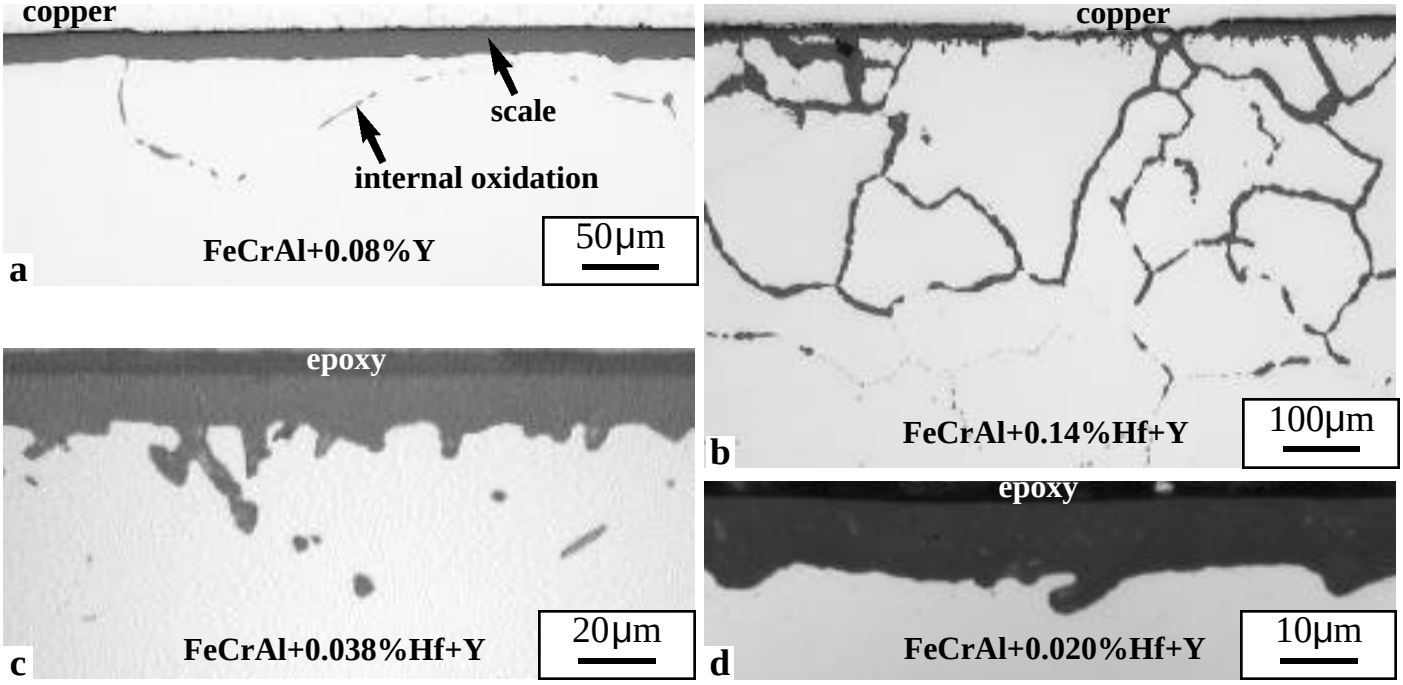

Figure 11. Light microscopy of the polished cross-section of the scale formed after 10, 100h cycles at 1200°C on FeCrAl with additions of (a) 0.08%Y (b) 0.14%Hf/Y (c) 0.038 Hf/Y and (d) 0.020%Hf/Y.

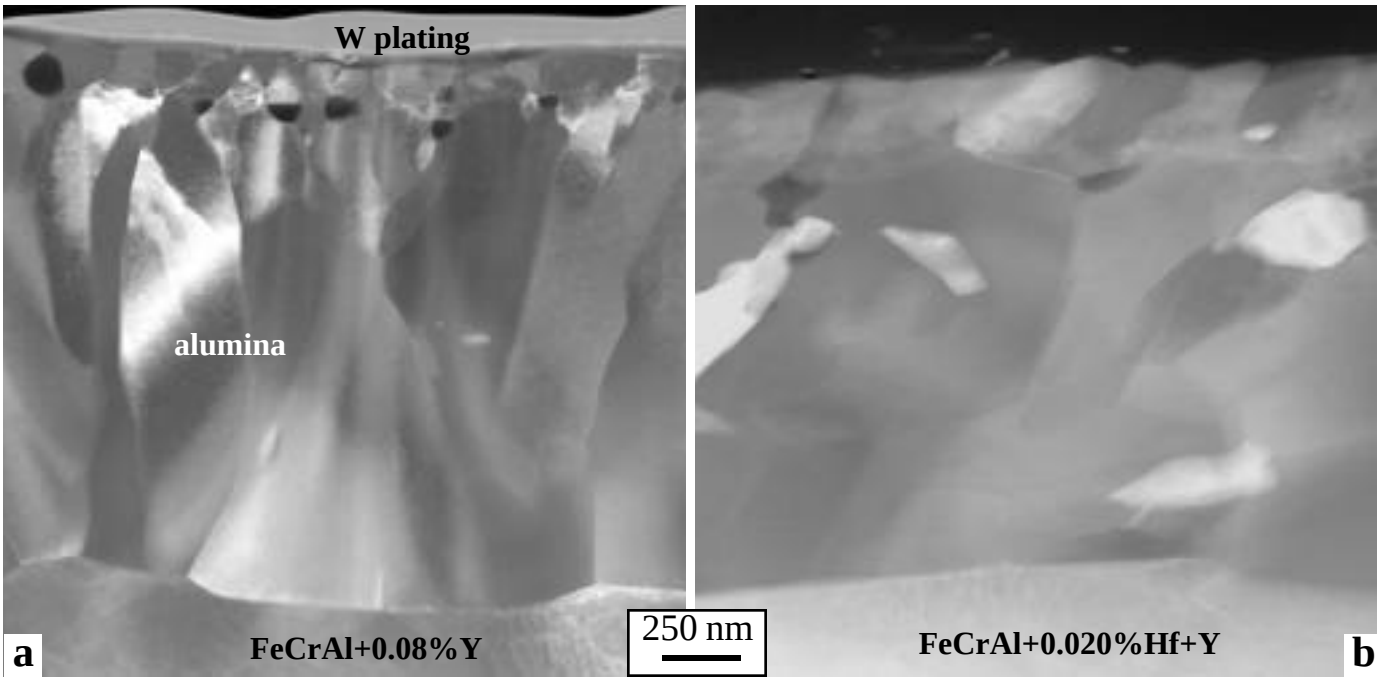

Figure 13. STEM annular dark field images of the scale formed after 2h at 1200°C on (a) FeCrAl+0.08Y and (b) FeCrAl +0.02%(Hf+Y)

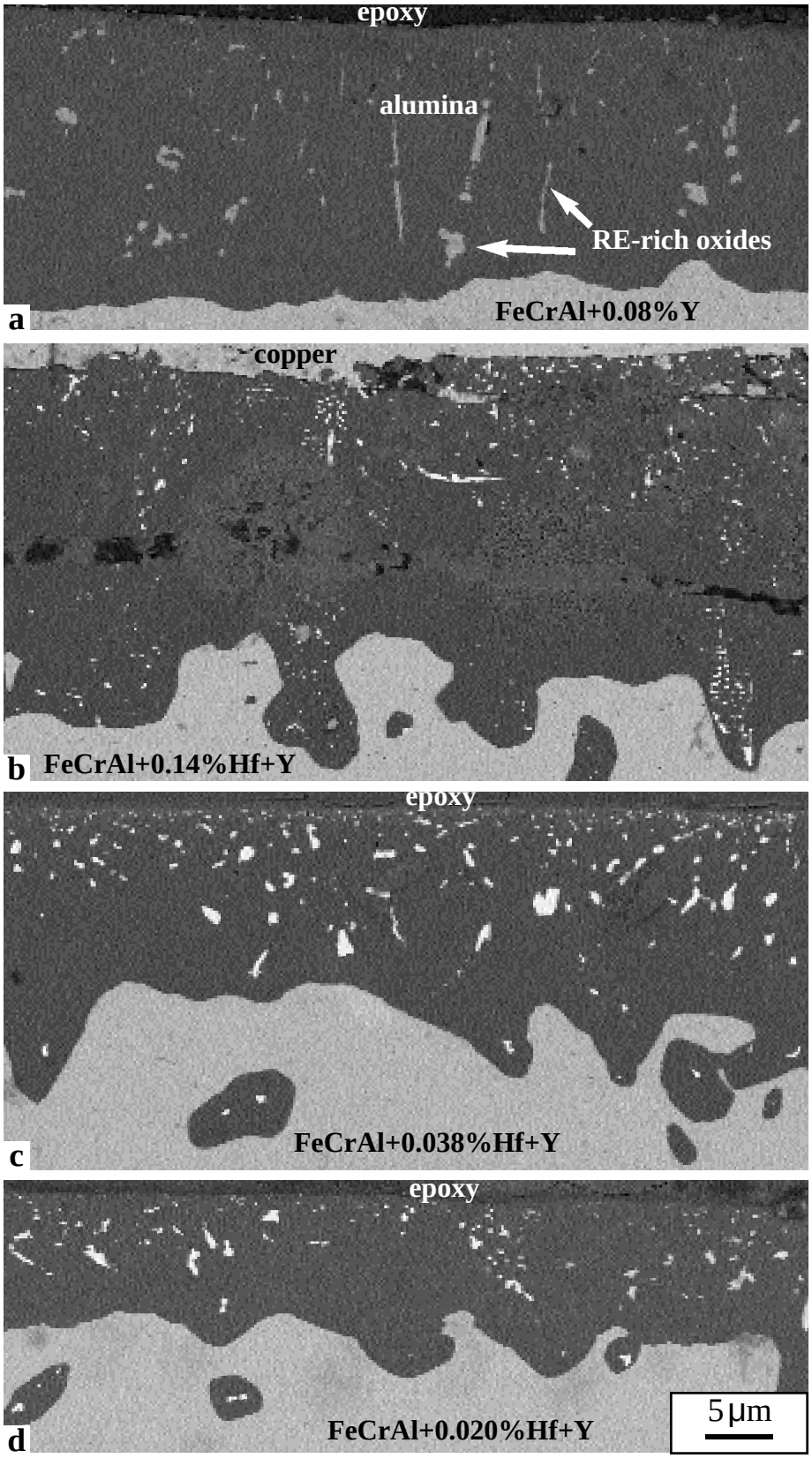

Figure 12. SEM back-scattered electron images of the polished cross-section of the scale formed after 10, 100h cycles at 1200°C on FeCrAl with additions of (a) 0.08%Y (b) 0.14%Hf/Y (c) 0.038 Hf/Y and (d) 0.020%Hf/Y.

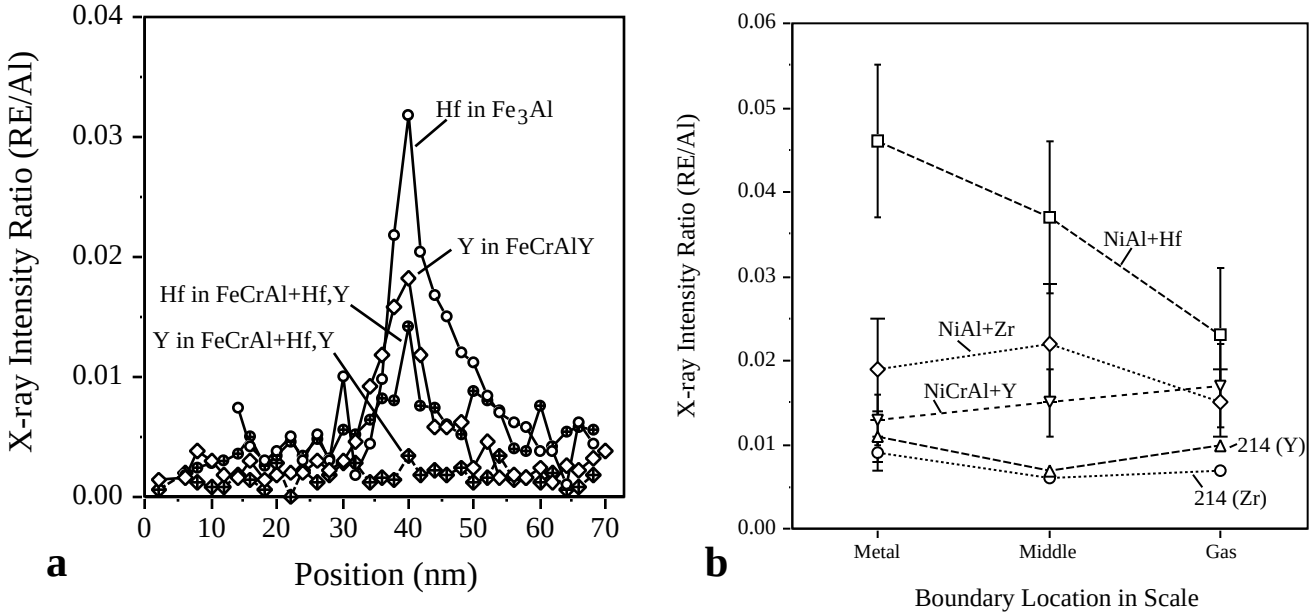

Figure 14. (a) Line scans across scale grain boundaries near the metal interface show the average relative x-ray intensities (RE/Al) for several Fe-base alloys oxidized for 2h at 1200°C. (b) Average peak grain boundary intensity ratios as a function of location in the alumina scale for Ni-base alloys oxidized for 100h at 1100°C.

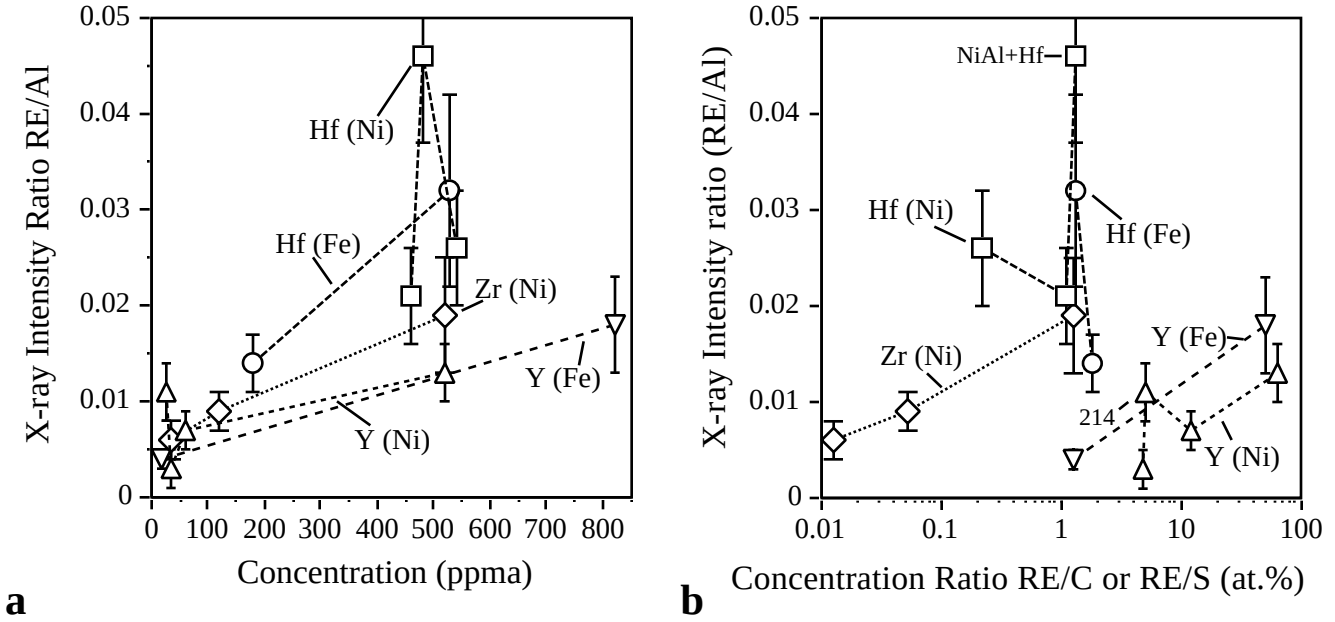

Figure 15. Average peak x-ray intensity ratios measured on scale grain boundaries near the metal-oxide interface in Fe-base and Ni-base alloys as a function of (a) RE concentration in the substrate alloy and (b) ratio of RE content to C or S content.

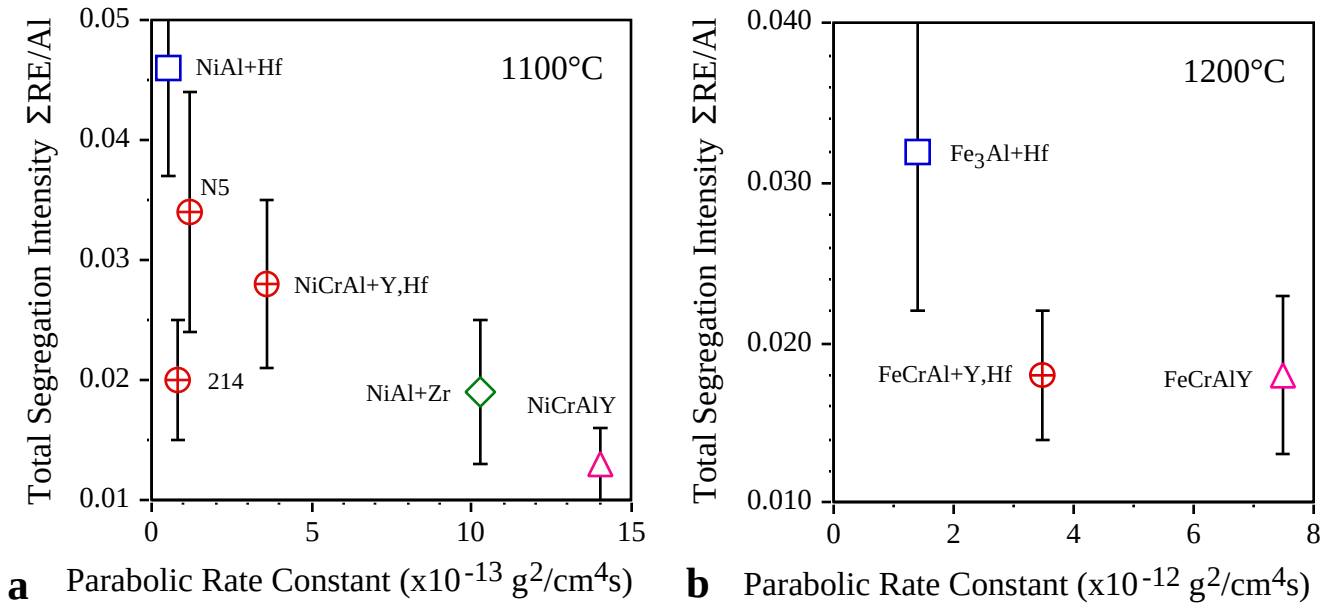

Figure 16. Average peak x-ray intensity ratios measured on alumina grain boundaries near the metal-scale interface versus the oxidation rate (a) for the Ni-base alloys at 1100°C and (b) for the Fe-base alloys at 1200°C.

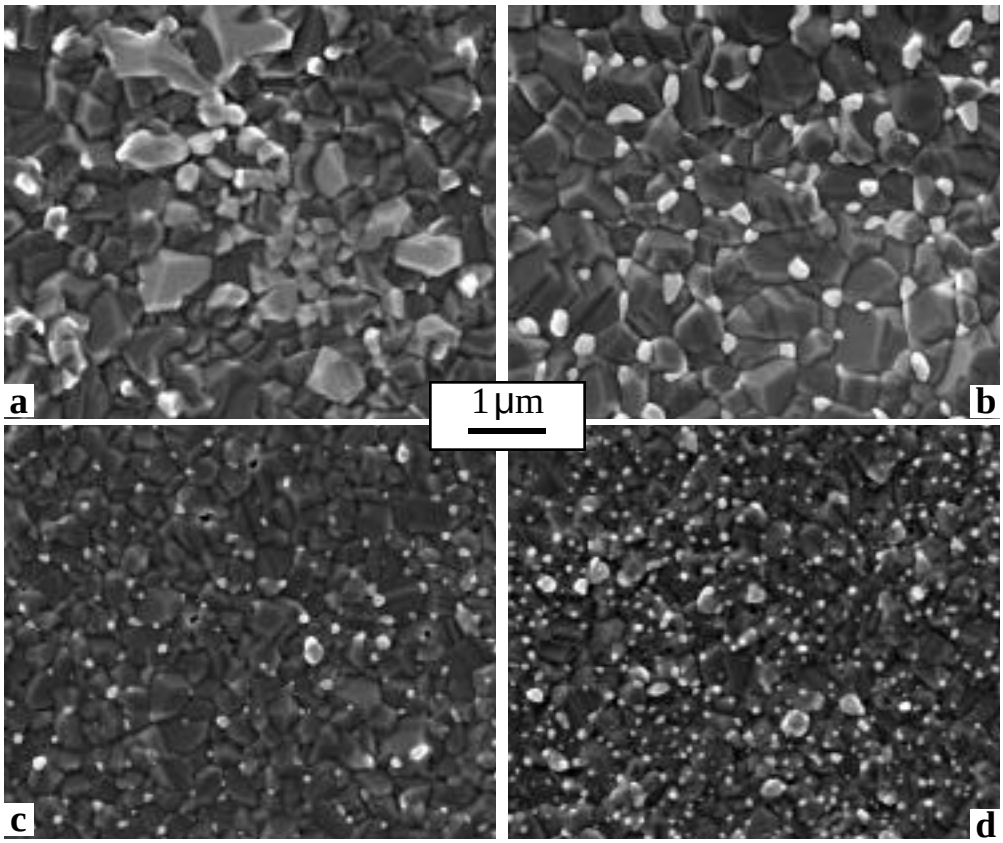

Figure 17. Plan view SEM secondary electron images of the scale formed after 10, 100h cycles at 1200°C on FeCrAl with additions of (a) 0.08%Y (b) 0.14%Hf/Y (c) 0.038 Hf/Y and (d) 0.020%Hf/Y.